Supplemental material

Nair et al., https://doi.org/10.1084/jem.20180118

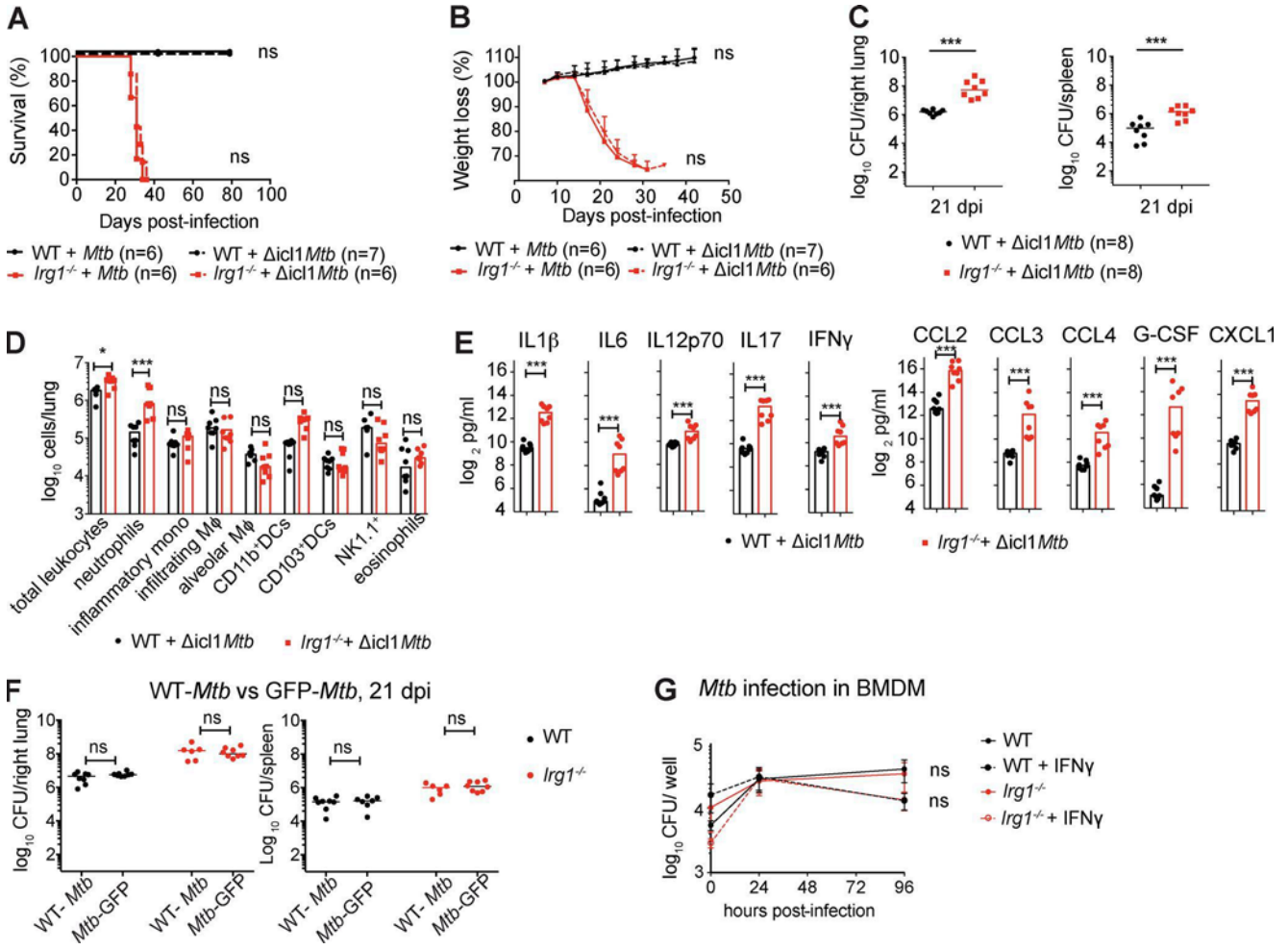

Figure S1. ***Irg1*$^{-/-}$ mice are susceptible to *Δicl1 Mtb* and infection of WT-*Mtb* or *Mtb*-GFP in WT and *Irg1*$^{-/-}$ mice and BMDMs.** Related to Figs. 1 and 2. **(A–E)** WT and *Irg1*$^{-/-}$ mice were infected with 100–200 CFU of aerosolized WT or isogenic *Δicl1 Mtb*. Mice were monitored for survival (A; *n* = 6–7), weight change (B; *n* = 6–7), and bacterial burden in the lung and spleen at 21 dpi (C; *n* = 8). Each point represents data from one mouse, and bars indicate median values. **(D)** Absolute numbers of myeloid cell populations in the lung were determined by flow cytometry at 21 dpi (*n* = 8). Mφ, macrophages. **(E)** Cytokine and chemokine levels at 21 dpi in lung homogenates were measured by a Bioplex-Pro cytokine assay (*n* = 8). **(F)** Comparison of WT-*Mtb* and *Mtb*-GFP burden in the lung and the spleen at 21 dpi (*n* = 6–8). Each point represents data from one mouse, and bars represent the median. No statistically significant differences were detected (Mann-Whitney test). **(G)** CFU analysis on *Mtb*-infected (multiplicity of infection of 1) WT and *Irg1*$^{-/-}$ BMDMs or IFN-γ pretreated WT and *Irg1*$^{-/-}$ BMDMs at 4, 24, and 96 h postinfection. Data in panel G are representative of three independent experiments. Statistical differences were determined by log-rank test (B), Mann-Whitney test (C-E), or one-way ANOVA with Tukey's correction (F and G; *, P < 0.05; ***, P < 0.001; ns, not significant).

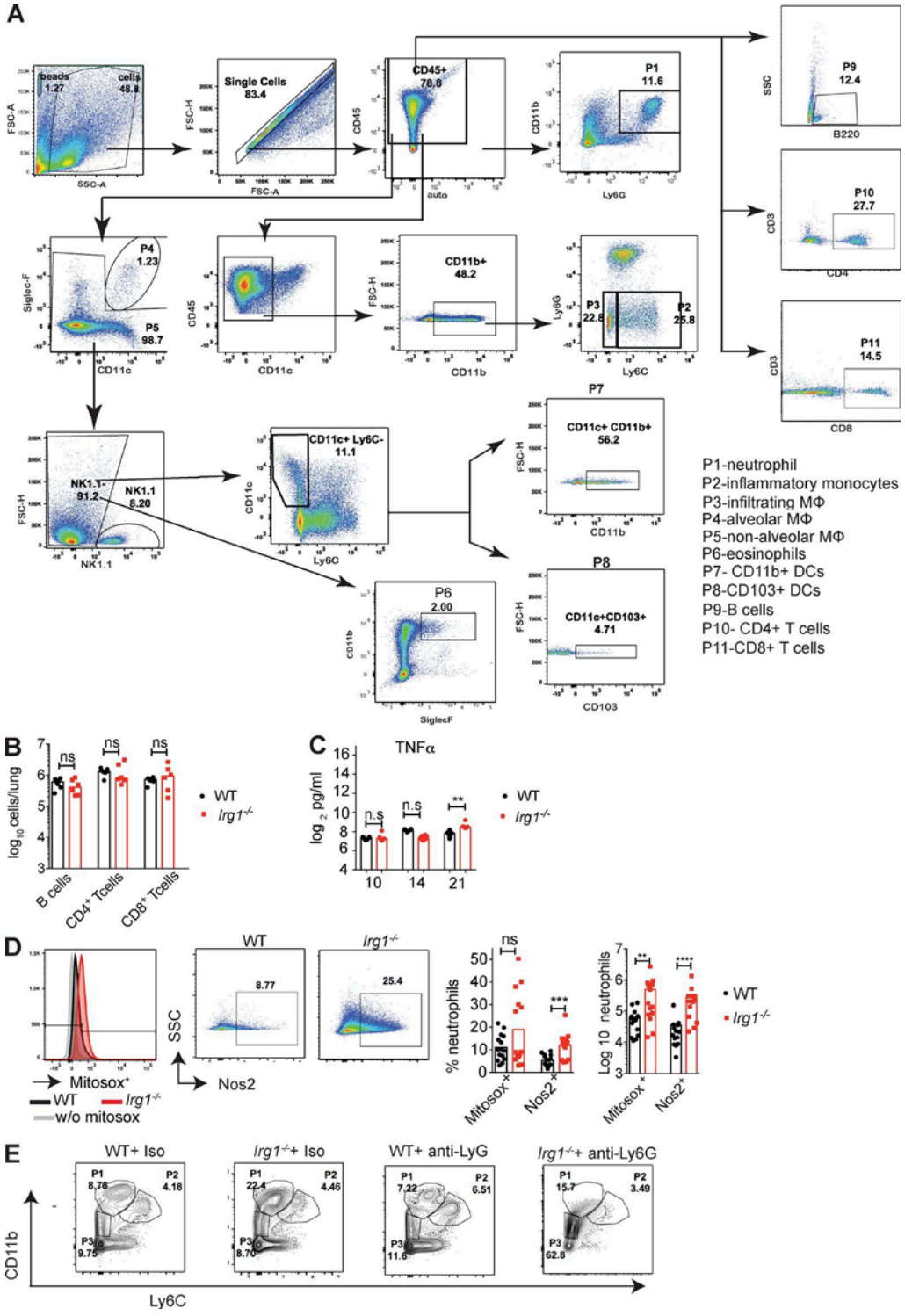

Figure S2. **Defining cellular infiltrates in the lungs of WT and *Irg1*$^{-/-}$ mice after *Mtb* infection and depletion of neutrophils.** Related to Figs. 2 and 4. **(A)** Gating strategy for analysis of innate immune cell populations in the lungs of *Mtb*-infected WT and *Irg1*$^{-/-}$ mice. **(B)** Absolute number of CD4$^+$ T cells, CD8$^+$ T cells, and B cells in the lungs of WT and *Irg1*$^{-/-}$ mice at 21 dpi (n = 6). Each point represents data from one mouse, and bars represent the median. **(C)** TNF-α concentrations were measured from lungs of WT and *Irg1*$^{-/-}$ mice by Bioplex-Pro cytokine assay at time points 10 dpi (n = 6), 14 dpi (n = 10), and 21 dpi (n = 6). **(D)** Mice were infected with *Mtb*-GFP. Representative histograms and flow cytometry plots for MitoSOX red$^+$ and Nos2$^+$ lung neutrophils in WT and *Irg1*$^{-/-}$ mice at 21 dpi. The percentage and number of MitoSOX red$^+$ and Nos2$^+$ lung neutrophils in WT and *Irg1*$^{-/-}$ mice at 21 dpi is shown. Each point represents data from one mouse, and bars represent the median. **(B–D)** Statistical differences were determined by the Mann-Whitney test (**, P < 0.01; ***, P < 0.001; ****, P < 0.0001; ns, not significant). SSC, side scatter. **(E)** Representative flow cytometry plots from two experiments confirming the extent of neutrophil depletion in the lungs of WT and *Irg1*$^{-/-}$ mice treated with anti-Ly6G mAb or an isotype control mAb at 21 dpi. All cells are CD45$^+$CD11c: P1-CD11b^{hi} Ly6C$^+$ neutrophils; P2-CD11b^{hi}Ly6C^{hi} inflammatory monocytes; and P3-CD11b^{low}LyC$^-$-infiltrating macrophages. Numbers on gates represent frequencies of CD45$^+$CD11c$^-$ cells.

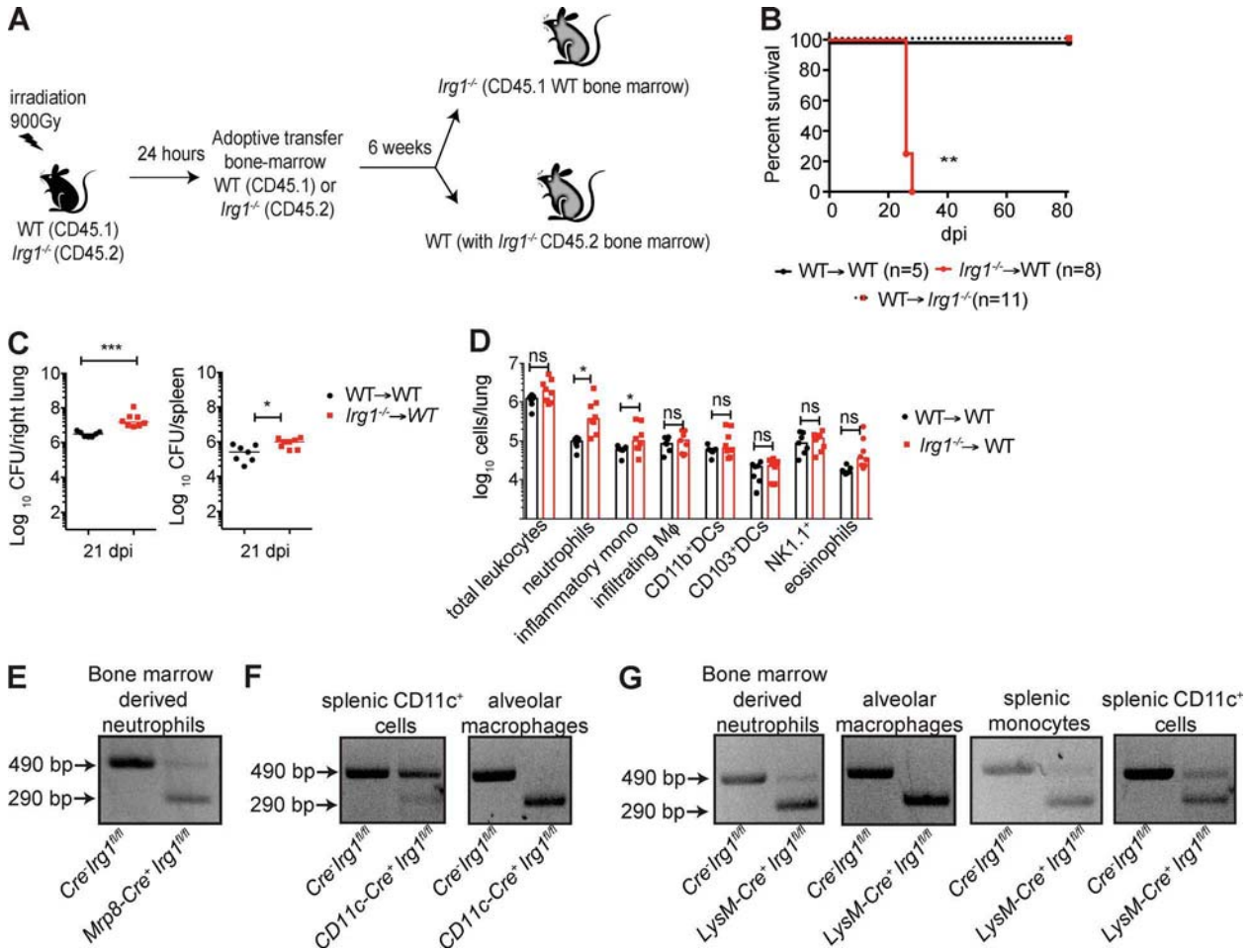

Figure S3. **Radiosensitive hematopoietic cells promote Irg1-mediated responses against *Mtb* and assessment of *Irg1* exon 4 deletion in conditional knock-out mice.** Related to Fig. 4. **(A)** Scheme for generation of bone marrow chimeric mice. **(B)** Survival of WT → WT, $Irg1^{-/-}$ → WT, and WT → $Irg1^{-/-}$ bone marrow chimeric mice infected with 100–200 CFU of aerosolized *Mtb*. The number of evaluated mice (*n*) is indicated in parentheses. **(C)** *Mtb* burden in the lung and spleen of bone marrow chimeric mice was measured at 21 dpi. **(D)** Absolute cell counts for WT (CD45.1) and $Irg1^{-/-}$ (CD45.2) innate immune cell populations within the lungs of chimeric mice as determined by flow cytometry at 21 dpi ($n = 7–8$). **(C–D)** Each point represents data from one mouse and bars indicate median values. All data are pooled from at least two independent experiments. Statistical differences were determined by log-rank test (**, $P < 0.01$; B) and Mann-Whitney tests (*, $P < 0.05$; ***, $P < 0.001$; ns, not significant; C and D). Mφ, macrophages. **(E–G)** Cells were isolated from $Irg1^{fl/fl}$ and $Irg1^{fl/fl}$ Cre–expressing mice. mRNA was then extracted and reverse transcribed, and a section of the *Irg1* gene spanning the exon 4 was amplified by PCR. Nonrecombined transcript yields a 490 bp amplicon, whereas Cre recombinase–mediated excision of exon 4 results in a 290 bp amplicon. **(E)** Recombined *Irg1* exon 4 in bone marrow neutrophils of *Cre*⁻ $Irg1^{fl/fl}$ and *Mrp8*-Cre⁺ $Irg1^{fl/fl\,f}$ mice. **(F)** Recombined *Irg1* exon 4 in total CD11c⁺ cells from spleens and alveolar macrophages from BAL fluid of *Cre*⁻ $Irg1^{fl/fl}$ and *CD11c*-Cre⁺ $Irg1^{fl/fl}$ mice. **(G)** Recombined *Irg1* exon 4 in bone marrow-derived neutrophils, alveolar macrophages isolated from BAL fluid, monocytes, and total CD11c⁺ cells from spleens of *Cre*⁻ $Irg1^{fl/fl}$ and *LysM*-Cre⁺ $Irg1^{fl/fl}$ mice.